Critical currents in graphene Josephson junctions

2008 J. Phys.: Condens. Matter 20 145218

(http://iopscience.iop.org/0953-8984/20/14/145218)

IOP PUBLISHING JOURNAL OF PHYSICS: CONDENSED MATTER

J. Phys.: Condens. Matter **20** (2008) 145218 (9pp) doi:10.1088/0953-8984/20/14/145218

Critical currents in graphene Josephson junctions

J González[1] **and E Perfetto**[2]

[1] Instituto de Estructura de la Materia, Consejo Superior de Investigaciones Científicas, Serrano 123, 28006 Madrid, Spain

[2] Consorzio Nazionale Interuniversitario per le Scienze Fisiche della Materia, Università di Roma Tor Vergata, Via della Ricerca Scientifica 1, 00133 Roma, Italy

Received 4 January 2008, in final form 21 February 2008
Published 19 March 2008
Online at stacks.iop.org/JPhysCM/20/145218

Abstract

We study the superconducting correlations induced in graphene when it is placed between two superconductors, focusing in particular on the supercurrents supported by the 2D system. For this purpose we make use of a formalism placing the emphasis on the many-body aspects of the problem, with the aim of investigating the dependence of the critical currents on relevant variables like the distance L between the superconducting contacts, the temperature, and the doping level. Thus we show that, despite the vanishing density of states at the Fermi level in undoped graphene, supercurrents may exist at zero temperature with a natural $1/L^3$ dependence at large L. When temperature effects are taken into account, the supercurrents are further suppressed beyond the thermal length L_T ($\sim v_F/k_B T$, in terms of the Fermi velocity v_F of graphene), entering a regime where the decay is given by a $1/L^5$ dependence. On the other hand, the supercurrents can be enhanced upon doping, as the Fermi level is shifted by a chemical potential μ from the charge neutrality point. This introduces a new crossover length $L^* \sim v_F/\mu$, at which the effects of the finite charge density start being felt, marking the transition from the short distance $1/L^3$ behavior to a softer $1/L^2$ decay of the supercurrents at large L. It turns out that the decay of the critical currents is given in general by a power-law behavior, which can be seen as a consequence of the perfect scaling of the Dirac theory applied to the low-energy description of graphene.

1. Introduction

Since the discovery of single atomic layers of carbon in 2004 [1], this new two-dimensional (2D) material (so-called graphene) has attracted a lot of attention [2]. From the experimental point of view, the 2D carbon sheets have shown a number of remarkable electronic properties. Thus, there has been evidence that graphene may have a finite lower bound ($4e^2/h$) in the conductivity at the charge neutrality point [3, 4]. Furthermore, an anomalous integer quantum Hall effect has been measured in the 2D system, with plateaus at odd-integer values of the quantum of conductance [3, 4]. The absence of weak localization effects [5] has also pointed to the unconventional effects that impurities and disorder in general may produce in the graphene sheet.

Most of the remarkable transport properties of graphene have to do with its particular band structure at low energies. The undoped system has a finite number of Fermi points, placed at the corners of the hexagonal Brillouin zone. Only two such points can be taken as independent, with quasiparticle excitations which have conical dispersion above and below the Fermi level [6]. This explains how the low-energy electronic states of graphene may be accommodated into two two-component spinor fields, governed by a Dirac Hamiltonian, which leads to a dispersion relation $\varepsilon(\mathbf{k}) = \pm v_F|\mathbf{k}|$. The electronic system displays hence a relativistic-like invariance at low energies, which is at the origin of the finite lower bound in the conductivity [7–10], the anomalous integer Hall effect [7, 11, 12], and the absence of backscattering in the presence of long-range scatterers [13]. Other exotic effects relying on the Dirac theory have been proposed, like the selective transmission of electrons through an n–p junction [14] or the specular Andreev reflection at a graphene–superconductor interface [15].

Recently, the properties of graphene have been also investigated when the material is placed between superconducting contacts. Thus, in the experiment reported in [16], it has been possible to measure supercurrents in graphene by attach-

ing wide superconducting electrodes with a spatial separation of ≈0.5 μm. In another experiment, reported in [17], a quite different geometry has been investigated by placing thin electrodes across a large 2D sample, with a minimum separation between the tips of ≈2.5 μm. In this case, the evidence of the superconducting correlations in graphene has been obtained in the form of Andreev reflection peaks in the I–V curves, as well as in the abrupt drop of the resistance at a temperature of ≈1 K, below the critical temperature (≈4 K) of the superconducting electrodes. Moreover, supercurrents have also been measured in the experiment reported in [18], where their development may have been favored by the large aspect ratio (∼10) between the width of the junction and the lead separation (of the order of a few hundred nanometers).

It is therefore pertinent to study the way in which the superconducting correlations are induced in graphene when it is placed between two superconductors, and how such correlations may depend on the geometry of the experimental setup. In this paper we are going to address this issue, focusing in particular on the supercurrents supported by the graphene sheet. We will be using a formalism placing the emphasis on the many-body aspects of the problem. This will allow us to clarify a number of questions, regarding the dependence of the critical currents on relevant variables like the distance between the superconducting contacts, the temperature, and the doping level of the graphene sample. In this respect, our approach can be seen as complementary to that of [19], where the Josephson effect has been studied in terms of Andreev reflection at superconducting contacts, concentrating on junctions with relatively short distance between the electrodes. We will be dealing with a framework where the tunneling and propagation of the Cooper pairs in graphene play the central role, placing in principle no restriction on the separation that may exist between superconducting contacts.

The content of this paper is organized as follows. We will set up in section 2 the formalism needed to describe the tunneling and propagation of Cooper pairs in graphene. This will be applied to the computation of the critical currents in section 3, where we will also discuss the different regimes depending on the interplay between the temperature and the distance between superconducting contacts. Section 4 will be devoted to extending our analysis to the case of finite doping, showing the enhancement experienced then by the supercurrents. Finally, we will summarize our results and draw our conclusions in section 5.

2. Model of graphene Josephson junction

Our purpose is to build a model that incorporates the low-energy properties of electron quasiparticles in graphene as well as the tunneling of electrons from graphene to the superconducting electrodes and vice versa. We take into account in particular that, below an energy scale of ∼1 eV, the electron dispersion relation has a conical shape, with a dependence of the energy ε on momentum $\mathbf{k}$ given by $\varepsilon(\mathbf{k}) \approx \pm v_{\mathrm{F}}|\mathbf{k}|$ [6]. We have to bear in mind that the 2D system has actually two independent Fermi points supporting such a conical dispersion, at opposite corners $K, -K$ of the hexagonal Brillouin zone. The dynamics of the quasiparticles in graphene can be therefore described in terms of a couple of two-component Dirac spinors $\Psi^{(a)}$, $a = 1, 2$, with a Hamiltonian [20, 21]

$$H_0 = v_{\mathrm{F}} \int \mathrm{d}^2 r \, \Psi_\sigma^{(a)\dagger}(\mathbf{r}) \, \boldsymbol{\sigma}^{(a)} \cdot \boldsymbol{\partial} \, \Psi_\sigma^{(a)}(\mathbf{r}) \tag{1}$$

where $\{\boldsymbol{\sigma}^{(a)}\}$ are two different suitable sets of Pauli matrices [11] (we use units such that $\hbar = 1$). In the above expression, the label of the spinor components is omitted for simplicity, and a sum is taken implicitly over the spin index σ as well as over the index a running over the two different low-energy valleys of the dispersion.

The above Hamiltonian has to be then complemented with a term accounting for the tunneling of electrons from the graphene side to the superconducting electrodes and vice versa. In this respect, we are going to assume that the tunneling takes place with equal amplitude for the two sublattices of the graphene honeycomb lattice. This kind of junction may be realized in cases where the contacts between graphene and the superconductors preserve the structure of the graphene lattice. From a technical point of view, such condition implies that the different spinor components and the different low-energy valleys couple with equal amplitude to the superconductors. By denoting the electron fields in the respective superconducting electrodes by Ψ_{S1} and Ψ_{S2}, we may write the tunneling Hamiltonian for contacts along the coordinates $x_1 = 0$ and $x_2 = L$ as

$$H_t = \sum_{j=1,2} t \int_0^W \mathrm{d}y \, \Psi_\sigma^{(a)\dagger}(x_j, y) \Psi_{Sj,\sigma}(x_j, y) + \mathrm{h.c.} \tag{2}$$

where the parameter t represents the tunneling amplitude. We stress at this point that, while the contacts have a width given by W in equation (2), the extension of the graphene layer along the transverse y direction is not constrained by this parameter in our model. Thus, our description will apply in general to 2D graphene samples, with dimensions in both the transverse and the longitudinal direction much larger than the contacts introduced by the superconducting electrodes.

The properties of the superconducting electrodes also have to be incorporated in the model of the Josephson junction. For the description of the supercurrents, it will be enough to specify the normal density of states ρ and the order parameter Δ in the superconducting state. We recall that a supercurrent arises in general from a gradient in the phase of the order parameter in a superconductor. In the case of a Josephson junction, the supercurrent is produced by a mismatch in the phases χ_1 and χ_2 of the respective order parameters in the superconducting electrodes. The Josephson current I_s is actually given by the derivative of the free energy with respect to the variable $\chi = \chi_1 - \chi_2$, and it can be therefore expressed as

$$I_s = 2e \frac{\partial}{\partial \chi} k_{\mathrm{B}} T \, \log\left(\mathrm{Tr}\, \mathrm{e}^{-H/k_{\mathrm{B}}T}\right) \tag{3}$$

where T is the temperature and H stands for the full Hamiltonian of the model.

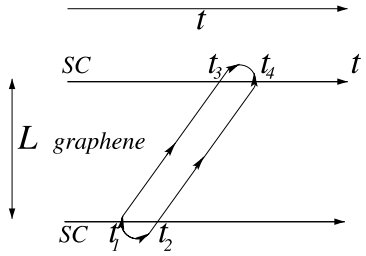

Figure 1. Schematic representation of the propagation of Cooper pairs in graphene between two superconductors (SCs).

In order to compute the Josephson current from equation (3), we will resort to a perturbative expansion in the tunneling amplitude t. The structure of the dominant contributions may however be very different depending on the actual geometry of the Josephson junction [22]. In cases where the distance L between the contacts is much smaller than the superconducting coherence length ξ, the supercurrents are built from processes with independent tunneling and uncorrelated propagation in graphene of the electrons of a Cooper pair. On the other hand, when L is much larger than ξ, the behavior is governed by the fast tunneling and subsequent propagation of the Cooper pair in graphene, as shown schematically in figure 1. This situation corresponds to the case where the time of propagation between the contacts is much larger than $1/|\Delta|$. Under the assumption of a large $|\Delta|$, the relevant properties of the superconductors may be encoded in the statistical average

$$\langle \Psi_{Sj,\sigma}(x_j, y; -\mathrm{i}\tau_1)\Psi_{Sj,-\sigma}(x_j, y; -\mathrm{i}\tau_2)\rangle \approx \mathrm{e}^{\mathrm{i}\chi_j}\rho\,\delta(\tau_1-\tau_2) \tag{4}$$

where the operators are ordered with respect to imaginary time τ.

From inspection of the expansion of the rhs in equation (3) in powers of the tunneling amplitude, we observe that the first nonvanishing contribution to I_s appears to fourth order in t, from a statistical average of operators participating of the condensates of the two superconductors. The expression of the maximum supercurrent I_c (critical current) is worked out at this perturbative level in the appendix, focusing on the regime corresponding to $L \gg \xi$. After factoring out the relative tunnel conductances at the contacts (given in each case by the dimensionless quantity $\rho t^2 W/v_F$), we end up with an expression for the behavior of the critical current intrinsic to the 2D graphene layer:

$$\begin{aligned} I_c^{(2D)}(T) \approx 2ev_F^2 &\int_0^W \mathrm{d}y_1 \int_0^W \mathrm{d}y_2 \\ &\times \int_0^{1/k_BT} \mathrm{d}\tau\, \langle \Psi_\uparrow^{(a)\dagger}(0, y_1; 0)\Psi_\downarrow^{(-a)\dagger}(0, y_1; 0) \\ &\times \Psi_\uparrow^{(b)}(L, y_2; -\mathrm{i}\tau)\Psi_\downarrow^{(-b)}(L, y_2; -\mathrm{i}\tau)\rangle. \end{aligned} \tag{5}$$

We observe from (5) that the propagator of the Cooper pairs evaluated over a distance L plays the central role in the determination of the supercurrents. We will study in what follows the behavior of this propagator depending on the distance L, the temperature, and the doping level.

3. Supercurrents at finite temperature

We analyze first the behavior of the supercurrents in graphene when the system is undoped, but is placed at a nonvanishing temperature T. The expectation values in the above formulas have to be understood then as statistical averages at this finite temperature. The building block for all the calculations is the electron propagator

$$G^{(a)}(\mathbf{r}, t) = -\mathrm{i}\langle T\Psi_\sigma^{(a)}(0, 0)\Psi_\sigma^{(a)\dagger}(\mathbf{r}, t)\rangle. \tag{6}$$

This is given in graphene by the propagator for Dirac fermions, corresponding to the Hamiltonian (1). In the many-body theory at temperature $T \neq 0$, the imaginary part of this object has a specific term to account for the thermal effects. The full expression of the Dirac propagator becomes in momentum space [23]

$$\begin{aligned} G^{(a)}(\mathbf{p}, \omega_p) = &\frac{\omega_p + \boldsymbol{\sigma}^{(a)}\cdot\mathbf{p}}{\omega_p^2 - \mathbf{p}^2 + \mathrm{i}\epsilon} \\ &+ \mathrm{i}2\pi(\omega_p + \boldsymbol{\sigma}^{(a)}\cdot\mathbf{p})\delta(-\omega_p^2 + \mathbf{p}^2)\frac{1}{1+\mathrm{e}^{|\omega_p|/k_BT}}. \end{aligned} \tag{7}$$

The Cooper-pair propagator in (5) can be computed from the convolution of two Dirac propagators, bearing in mind that they correspond to fields at opposite valleys of the graphene dispersion. In doing this operation, we will also have to be consistent with our assumption that the tunneling at the superconducting contacts is the same for the two sublattices of the graphene lattice. This means that, when taking the average for the Cooper-pair propagator, we will also take a trace in spinor space over the states of the Cooper pairs in sublattice A, given by $\Psi_{A,\uparrow}^{(a)}(\mathbf{k}+\mathbf{q})\Psi_{A,\downarrow}^{(-a)}(-\mathbf{q})$, and in sublattice B, given by $\Psi_{B,\uparrow}^{(a)}(\mathbf{k}+\mathbf{q})\Psi_{B,\downarrow}^{(-a)}(-\mathbf{q})$. The Cooper-pair propagator thus defined in momentum space, $D(\mathbf{k}, \omega)$, can be expressed as

$$\begin{aligned} D(\mathbf{k}, \omega_k) = \mathrm{i}\,\mathrm{Tr}\int &\frac{\mathrm{d}\omega_q}{2\pi} \\ \times \int &\frac{\mathrm{d}^2q}{(2\pi)^2} G^{(a)}(\mathbf{q}+\mathbf{k}, \omega_q+\omega_k)G^{(-a)}(-\mathbf{q}, -\omega_q). \end{aligned} \tag{8}$$

A nice feature of the diagrammatics of the many-body theory at $T \neq 0$ is that the terms carrying the dependence on temperature do not need to be regularized by means of a high-energy cutoff. The contributions at $T = 0$, however, remain finite only when the integrals over the momenta are suitably cut off. In the present model, it is convenient to choose a method of regularization of the integrals preserving the relativistic-like invariance of the theory. For this purpose, we will adopt an analytic continuation in the number of space–time dimensions [24], that is, carrying out first the integrals at general dimension D, and then taking the limit $D \to 3$. To implement this procedure, we first collect the components of the momentum and the frequency to form 3D vectors, $q \equiv (v_F\mathbf{q}, \omega_q)$, $k \equiv (v_F\mathbf{k}, \omega_k)$. Next, we may rotate all the 3D vectors to Euclidean space by introducing imaginary frequencies, $\overline{\omega}_q = -\mathrm{i}\omega_q$. One can easily see that the expression of the propagator (8) at general dimension D becomes

$$D(\mathbf{k}, \mathrm{i}\overline{\omega}_k)|_{T=0} = \int_0^1 \mathrm{d}x \int \frac{\mathrm{d}^Dq}{(2\pi)^D} \frac{2q^2 - 2k^2x(1-x)}{\left(q^2 + k^2x(1-x)\right)^2}$$

$$= \left(\frac{1}{4\pi^{3/2}}\Gamma\left(1-\frac{D}{2}\right) - \frac{1}{2\pi^{3/2}}\Gamma\left(2-\frac{D}{2}\right)\right) \times \int_0^1 \mathrm{d}x \sqrt{k^2 x(1-x)}. \quad (9)$$

In the last passage we have made use of standard formulas in dimensional regularization. Quite remarkably, the result turns out to be finite in the limit $D \to 3$. After reverting the rotation back to real frequency, we finally get

$$D(\mathbf{k}, \omega)|_{T=0} = -\frac{1}{8v_\mathrm{F}^2}\sqrt{v_\mathrm{F}^2\mathbf{k}^2 - \omega^2}. \quad (10)$$

The part of the Cooper-pair propagator depending on temperature can be computed by using the second term in (7) to make the convolution (8). For our purposes, we can concentrate on the calculation of the Cooper-pair propagator at zero frequency. By adding the result (10) to the temperature-dependent contribution, we get

$$D(\mathbf{k}, 0) = -\frac{1}{8v_\mathrm{F}}|\mathbf{k}| - \frac{\log(2)}{\pi v_\mathrm{F}^2}k_\mathrm{B}T + \frac{1}{2\pi v_\mathrm{F}}|\mathbf{k}|\int_0^1 \mathrm{d}x\, \frac{1}{\sqrt{1-x^2}}\frac{1}{1+\mathrm{e}^{xv_\mathrm{F}|\mathbf{k}|/2k_\mathrm{B}T}}. \quad (11)$$

From the results (10) and (11), we can already extract a number of conclusions regarding the behavior of the supercurrents in long graphene Josephson junctions. From equation (5), we can express the critical current for $L \gg W$ as

$$I_\mathrm{c}^{(2\mathrm{D})}(T) \approx 2ev_\mathrm{F}^2W^2\int_0^\infty \frac{\mathrm{d}k}{2\pi}\,|\mathbf{k}|\,J_0(|\mathbf{k}|L)D(\mathbf{k},0)\mathrm{e}^{-|\mathbf{k}|/k_\mathrm{c}}. \quad (12)$$

A short distance cutoff k_c has been introduced to regularize the integral over the momentum. This is actually justified on physical grounds, since the description of graphene as a continuum in terms of the Dirac theory makes sense at distances above the nanometer scale. A sensible choice corresponds to $v_\mathrm{F}k_\mathrm{c} \sim 1$ eV. We will see that, at distances such that $L \gg k_\mathrm{c}^{-1}$, the behavior of the critical current is in general not sensitive to the actual value of the cutoff.

At $T = 0$, the dependence of the critical current on L can be obtained from the Cooper-pair propagator (10). Actually, we can derive an analytical expression for $I_\mathrm{c}^{(2\mathrm{D})}(0)$ by computing the integral in (12):

$$I_\mathrm{c}^{(2\mathrm{D})}(0) \sim -ev_\mathrm{F}W^2\int_0^\infty \mathrm{d}k\,|\mathbf{k}|^2\,J_0(|\mathbf{k}|L)\mathrm{e}^{-|\mathbf{k}|/k_\mathrm{c}} \quad (13)$$

$$= ev_\mathrm{F}W^2\frac{k_\mathrm{c}^3(k_\mathrm{c}^2L^2-2)}{\sqrt{(k_\mathrm{c}^2L^2+1)^5}}. \quad (14)$$

From this result we check that, as expected, the behavior of the critical current is not affected by the cutoff k_c in the limit of large L. In this regime we find

$$I_\mathrm{c}^{(2\mathrm{D})}(0) \sim ev_\mathrm{F}W^2\frac{1}{L^3}. \quad (15)$$

The strong power-law decay shown by (15) can be understood actually as a reflection of the linear dependence on momentum of the quasiparticle energy, which dictates in turn the behavior of the Cooper-pair propagator (10) [25]. We reach anyhow the interesting conclusion that, while graphene has a vanishing density of states at the Dirac point, it may still support a nonvanishing supercurrent when the Fermi level is at this charge neutrality point.

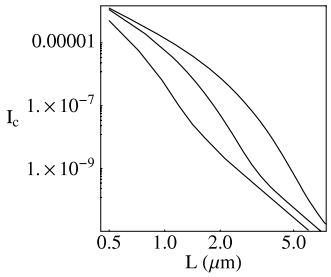

Figure 2. Logarithmic plot of the critical current $I_\mathrm{c}^{(2\mathrm{D})}$ (in units of $10^{-2}ev_\mathrm{F}k_\mathrm{c} \approx 1.2\ \mu$A) as a function of the distance L, taking $W = 10^2/k_\mathrm{c}$ (=50 nm). The three curves correspond, from top to bottom, to different values of the temperature $T = 2$, 4, and 8 K.

The inspection of the full propagator (11) also reveals that the scaling is drastically modified when $k_\mathrm{B}T \gg v_\mathrm{F}|\mathbf{k}|$. Actually, we can distinguish between a high-temperature and a low-temperature regime of the Cooper-pair propagator, with quite different behaviors:

$$D(\mathbf{k}, 0) \approx -\frac{1}{8v_\mathrm{F}}|\mathbf{k}| \qquad \text{if } k_\mathrm{B}T \ll v_\mathrm{F}|\mathbf{k}| \quad (16)$$

$$\approx -\frac{\log(2)}{\pi v_\mathrm{F}^2}k_\mathrm{B}T - \frac{1}{16\pi}\frac{|\mathbf{k}|^2}{k_\mathrm{B}T} \qquad \text{if } k_\mathrm{B}T \gg v_\mathrm{F}|\mathbf{k}|. \quad (17)$$

The existence of this crossover in the momentum gives rise to an abrupt decay of the supercurrent beyond the thermal length $L_T = v_\mathrm{F}/k_\mathrm{B}T$. This is illustrated in figure 2, where the critical current $I_\mathrm{c}^{(2\mathrm{D})}(T)$ is represented as a function of the distance L at different temperatures. We observe for instance that, for a temperature of the order of $T \sim 1$ K, the scale of the crossover in L is of the order of a few microns, in agreement with the expression of the thermal length.

From a physical point of view, it becomes clear that the Cooper pairs do not feel the thermal effects during their propagation when L is shorter than the scale given by L_T, while they are increasingly disrupted at distances larger than the thermal length. At short distances such that $L \ll v_\mathrm{F}/k_\mathrm{B}T$, the decay of the critical current represented in figure 2 follows a $1/L^3$ power-law, in agreement with the above analysis at $T = 0$. However, beyond the crossover clearly identified in the three curves, we see that a different power-law behavior opens up at long distance $L \gg v_\mathrm{F}/k_\mathrm{B}T$. This regime can be analyzed by considering that, when T is very large, the second term in the approximation (17) dictates the long distance decay of the critical current. In this case we can compute again analytically the integral in (12):

$$I_\mathrm{c}^{(2\mathrm{D})}(T) \sim -ev_\mathrm{F}^2W^2\frac{1}{k_\mathrm{B}T}\int_0^\infty \mathrm{d}k\,|\mathbf{k}|^3\,J_0(|\mathbf{k}|L)\mathrm{e}^{-|\mathbf{k}|/k_\mathrm{c}} \quad (18)$$

$$= ev_\mathrm{F}W^2\frac{v_\mathrm{F}}{k_\mathrm{B}T}\frac{k_\mathrm{c}^4(9k_\mathrm{c}^2L^2-6)}{\sqrt{(k_\mathrm{c}^2L^2+1)^7}}. \quad (19)$$

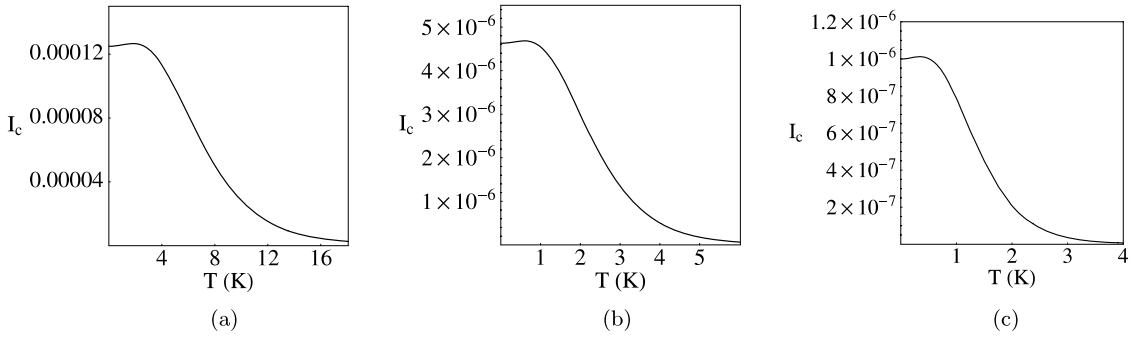

Figure 3. Plot of the critical current $I_c^{(2D)}(T)$ (in units of $10^{-2} e v_F k_c \approx 1.2\ \mu$A) as a function of the temperature, for $W = 10^2/k_c$ (=50 nm) and a spatial separation between superconducting contacts $L = 0.5\ \mu$m (a), 1.5 μm (b), and 2.5 μm (c).

The leading contribution to the critical current becomes then for $L \gg v_F/k_B T$

$$I_c^{(2D)}(T) \sim e v_F W^2 \frac{v_F}{k_c k_B T} \frac{1}{L^5}. \tag{20}$$

The existence of this stronger power-law decay is manifest in the results of the numerical computation of the critical current represented in figure 2, as it can be checked that the rightmost part of the lower curves in the plot corresponds with great accuracy to a power-law behavior with the exponent given by equation (20).

In order to establish a comparison with experimental results, the relevant behavior is given by the critical current represented as a function of the temperature at fixed length L. The existence of a thermal length has a reflection here in the form of a crossover temperature T^*, which marks the strong decay of the critical current for $T > T^*$. We have plotted in figure 3 the critical current $I_c^{(2D)}(T)$, computed from equation (12), at different values of L between 0.5 μm and 2.5 μm. The shapes of the curves in the figure are quite similar, and it can be checked that they can be collapsed into a single universal curve after rescaling the temperature by $T^* \propto v_F/k_B L$, as shown in figure 4. This is consistent with the expression of the critical current in equation (12), where it is seen that the effect of a variation of the length L on $I_c^{(2D)}(T)/I_c^{(2D)}(0)$ can be compensated by a suitable change in the scale of T, in the regime where the critical current is not sensitive to the precise value of k_c.

We observe that the behavior of the critical current is in all cases quite stable for $T \ll T^*$ and that there is even an upturn before the abrupt drop at the crossover temperature. These features have also been found in the theoretical investigation of the supercurrents in one-dimensional (1D) electron systems [22] and in carbon nanotubes [26]. The shape of the critical currents obtained there is qualitatively similar to that of the curves in figure 3. A major difference is however that the decay of the supercurrents in the carbon nanotubes is given by a $1/L$ dependence in the ballistic regime, instead of the much stronger power-law decay (15) in graphene.

It is worth mentioning at this point the experiment reported in [17], in which the properties of a graphene Josephson junction have been measured in the regime of large distance between superconducting electrodes. In the experimental setup described there, the minimum distance between superconducting contacts can be estimated as $\approx$ 2.5 μm. While no supercurrent was observed below the critical temperature T_c of the electrodes ($\approx$4 K), a signature of the proximity effect was obtained in the measurements of the resistance as a function of temperature, in the form of a sharp decrease at $T \approx 1$ K. Quite remarkably, this value of T is in good correspondence with the crossover temperature that we find in our model for a distance $L = 2.5\ \mu$m, as can be seen from figure 3(c). It is therefore likely that the sharp decrease measured in the resistance has its origin in the same suppression of the thermal effects as enhances the supercurrents at $T < T^*$. We also notice that the prediction from our model is that the critical currents for such a large value of L should be well below the scale of 1 nA. This may explain the failure to establish a supercurrent in the experiment of [17], and it may also anticipate better perspectives in experiments with suitably short graphene junctions.

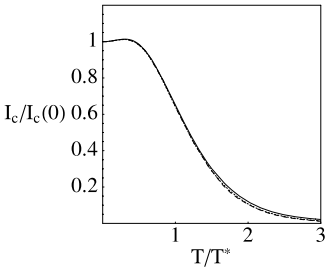

Figure 4. Combined plot of $I_c^{(2D)}(T)/I_c^{(2D)}(0)$ represented as a function of the scaled variable T/T^* (with $T^* = v_F/2L$), where the collapse of the three curves corresponding to values of the distance $L = 0.5\ \mu$m (full line), 1.5 μm (dotted line), and 2.5 μm (dashed line) is seen.

4. Supercurrents at finite doping

We have seen that the origin of the relative smallness of the critical currents in undoped graphene lies in the vanishing density of states at the Dirac point. Therefore, a straightforward way to enhance the supercurrents may simply consist in shifting the Fermi level away from the charge neutrality point, as shown in figure 5. In practice, this can

Figure 5. Schematic representation of the two independent Dirac valleys at the corners of the hexagonal Brillouin zone, showing the regions of occupied (dark) and unoccupied (white) energy levels in doped graphene.

(This figure is in colour only in the electronic version)

be achieved by doping the graphene sheet. In our theoretical framework, we will assume that this effect can be accounted for by means of a finite chemical potential μ. Thus, the Hamiltonian for the graphene part of the junction will now read

$$H_0 = \int \mathrm{d}^2 r\, \Psi_\sigma^{(a)\dagger}(\mathbf{r}) \left(v_\mathrm{F} \boldsymbol{\sigma}^{(a)} \cdot \boldsymbol{\partial} - \mu \right) \Psi_\sigma^{(a)}(\mathbf{r}). \tag{21}$$

Working at $\mu \neq 0$ leads to significant modifications in the propagator of the Dirac fermions and in the Cooper-pair propagator. The Dirac propagator corresponding to the Hamiltonian (21) turns out to be (for $\mu > 0$) [27]

$$G^{(a)}(\mathbf{k}, \omega) = (\omega + v_\mathrm{F} \boldsymbol{\sigma}^{(a)} \cdot \mathbf{k}) \left[\frac{1}{\omega^2 - v_\mathrm{F}^2 \mathbf{k}^2 + \mathrm{i}\epsilon} + \mathrm{i}\pi \frac{\delta(\omega - v_\mathrm{F}|\mathbf{k}|)}{v_\mathrm{F}|\mathbf{k}|} \theta(\mu - v_\mathrm{F}|\mathbf{k}|) \right]. \tag{22}$$

As shown in the appendix, the representation (22) is nothing but a compact form of expressing the propagation of quasiparticles with $v_\mathrm{F}|\mathbf{k}| > \mu$ and quasiholes with $\pm v_\mathrm{F}|\mathbf{k}| < \mu$, in the particular case of conical dispersion.

The propagator (22) is very convenient to carry out calculations in the many-body theory and, in particular, it allows us to compute the dependence on μ of the Cooper-pair propagator as a correction to the expression (10) at $\mu = 0$. In this procedure, we observe that the second term in the rhs of (22) does not introduce any integrals requiring regularization in the diagrammatics of the Dirac theory. By computing then the Cooper-pair propagator according to equation (8), we obtain [25]

$$D(\mathbf{k}, 0) = \begin{cases} -\dfrac{1}{2\pi v_\mathrm{F}^2}\mu & \text{if } v_\mathrm{F}|\mathbf{k}| < 2\mu \\ -\dfrac{1}{8 v_\mathrm{F}}|\mathbf{k}| + \dfrac{1}{4\pi v_\mathrm{F}}|\mathbf{k}| \arcsin\left(\dfrac{2\mu}{v_\mathrm{F}|\mathbf{k}|}\right) - \dfrac{1}{2\pi v_\mathrm{F}^2}\mu & \\ \qquad\qquad \text{if } v_\mathrm{F}|\mathbf{k}| > 2\mu. \end{cases} \tag{23}$$

At large values of $v_\mathrm{F}|\mathbf{k}| \gg \mu$, we recover from (23) the linear dependence on the momentum that is characteristic of the Cooper-pair propagator in the undoped system. However, the chemical potential introduces a clear deviation from this behavior at small $|\mathbf{k}|$, which has significant consequences in the decay of the supercurrent at long distances. This is illustrated in figure 6, where the existence in general of a crossover length scale L^* mediating the transition towards a softer power-law decay can be appreciated.

According to (23), we can express the critical current $I_\mathrm{c}^{(2\mathrm{D})}(0)$ at finite chemical potential in the form

$$I_\mathrm{c}^{(2\mathrm{D})}(0) = I_{\mathrm{c}1}^{(2\mathrm{D})}(0) + I_{\mathrm{c}2}^{(2\mathrm{D})}(0) \tag{24}$$

with

$$I_{\mathrm{c}1}^{(2\mathrm{D})}(0) = -\frac{1}{\pi} e W^2 \mu \int_0^\infty \frac{\mathrm{d}k}{2\pi}\, |\mathbf{k}|\, J_0(|\mathbf{k}|L) \mathrm{e}^{-|\mathbf{k}|/k_\mathrm{c}} \tag{25}$$

$$I_{\mathrm{c}2}^{(2\mathrm{D})}(0) = -\frac{1}{2\pi} e v_\mathrm{F} W^2 \times \int_{2\mu/v_\mathrm{F}}^\infty \frac{\mathrm{d}k}{2\pi}\, |\mathbf{k}|^2 \arccos\left(\frac{2\mu}{v_\mathrm{F}|\mathbf{k}|}\right) J_0(|\mathbf{k}|L) \mathrm{e}^{-|\mathbf{k}|/k_\mathrm{c}}. \tag{26}$$

The first contribution to (24) is not relevant, since we have

$$I_{\mathrm{c}1}^{(2\mathrm{D})}(0) = -\frac{1}{\pi} e W^2 \mu \frac{k_\mathrm{c}^2}{\sqrt{(k_\mathrm{c}^2 L^2 + 1)^3}} \tag{27}$$

which is smaller than the estimate (15) at $\mu = 0$ by a factor $\mu / v_\mathrm{F} k_\mathrm{c}$. The second contribution may however change the behavior of the critical current at large L, as the integrand is not analytic at $|\mathbf{k}| = 2\mu/v_\mathrm{F}$. The expression for $I_{\mathrm{c}2}^{(2\mathrm{D})}(0)$ is actually finite in the limit $k_\mathrm{c} \to \infty$, and we obtain

$$I_{\mathrm{c}2}^{(2\mathrm{D})}(0) \sim -e v_\mathrm{F} W^2 \frac{\mu^3}{v_\mathrm{F}^3} \times \int_1^\infty \mathrm{d}x\, x^2 \arccos\left(\frac{1}{x}\right) J_0((2\mu L/v_\mathrm{F})x) \tag{28}$$

$$\sim e W^2 \mu \frac{1}{L^2} \qquad \text{for } \mu L / v_\mathrm{F} \gg 1. \tag{29}$$

We have to stress anyhow that $I_{\mathrm{c}2}^{(2\mathrm{D})}(0)$ has oscillations as a function of L, arising from the behavior of the Bessel function J_0. The power-law decay (29) applies then to the envelope of the maxima of the critical current, as illustrated in figure 6(a). There the crossover from the $1/L^3$ behavior to the oscillatory regime with softer power-law decay can be appreciated. From the numerical results represented in the figure, it can be checked that the $1/L^2$ behavior is followed with great accuracy at large values of L (compared to v_F/μ).

From a practical point of view, the most important result that we obtain is the significant enhancement of the critical currents at moderate values of the chemical potential. This is clearly observed in the plots of figure 6, where the crossover to the $1/L^2$ decay is always found at a length scale consistent with the theoretical estimate $L^* \sim v_\mathrm{F}/\mu$. For a chemical potential $\mu \approx 10$ meV, for instance, this scale is $\approx$50 nm. The critical currents can be then enhanced to values above the nanoampere scale for spatial separation between superconducting contacts $L \gtrsim 500$ nm (assuming thin electrodes as in our case with $W \sim 50$ nm). This should open good perspectives to establish supercurrents in graphene Josephson junctions by suitable doping of the samples.

5. Conclusion

In this paper we have adopted a framework suited to address the many-body properties of graphene Josephson junctions. We have described the development of the supercurrents through the tunneling and propagation of Cooper pairs in the graphene part of the junction, with the aim of investigating the dependence of the critical currents on relevant variables like the distance between the superconducting contacts, the temperature, and the doping level. We have been able

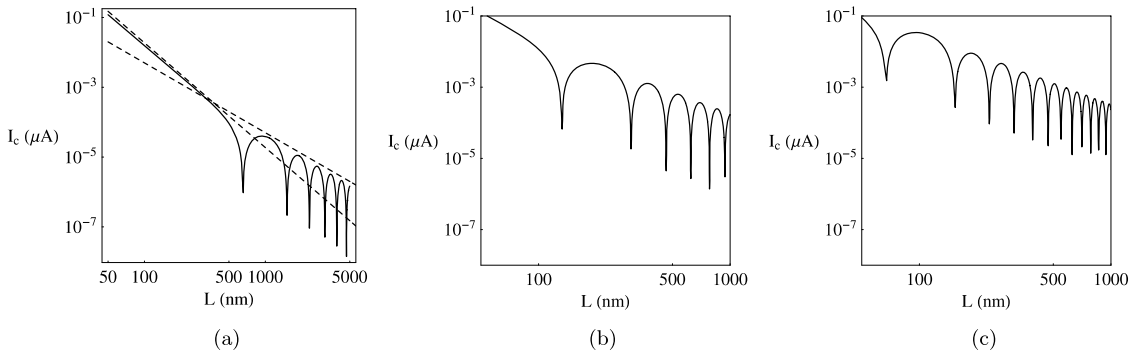

Figure 6. Plot of the zero-temperature critical current $I_c^{(2D)}(0)$ as a function of the distance L, for $W = 10^2/k_c$ (=50 nm) and three different values of the chemical potential $\mu = 1$ meV (a), 5 meV (b), and 10 meV (c). The dashed straight lines in figure 3(a) are drawn as a reference to the power-law dependences $1/L^3$ and $1/L^2$.

then to characterize different regimes in the behavior of the supercurrents, depending on the relation between these variables.

The supercurrents have a natural tendency to decay in the graphene part of the Josephson junction, following in general a power-law behavior with respect to the distance L between the superconducting contacts. Such a power-law decay is particularly strong in undoped graphene, given the vanishing density of states at the charge neutrality point. We have shown that the critical currents display then at zero temperature a $1/L^3$ dependence on the distance L. When temperature effects are taken into account, there is always a finite thermal length L_T (of the order of $\sim v_F/k_B T$) beyond which the supercurrents are further suppressed, due to the disruption of the Cooper pairs by many-body effects. When this takes place, the supercurrents enter a regime where the natural decay is given by a $1/L^5$ dependence.

On the other hand, many-body effects can also be used to our benefit to enhance the critical currents, in this case by shifting the Fermi level away from the charge neutrality point. This can be achieved in our framework by means of a chemical potential $\mu \neq 0$. Inducing in this way a finite density of states at the Fermi level, we have seen that the critical currents are enhanced beyond a new crossover length $L^* \sim v_F/\mu$. This is actually the scale at which the effects of the finite charge density start being felt, marking the transition from the previously discussed $1/L^3$ behavior to a softer $1/L^2$ decay of the supercurrents at long distances.

At this point, it is interesting to note that the $1/L^3$ decay at zero temperature in undoped graphene is similar to the behavior found in the investigation of mesoscopic junctions made of a diffusive metal [28]. In this case, the product of the critical current times the normal resistance of the metal is proportional to the Thouless energy, which depends on length L as $1/L^2$. This implies consequently a $1/L^3$ decay of the critical current, which we have seen is characteristic of graphene under conditions of ballistic transport. The reminiscence of some of the properties of clean graphene with respect to the behavior of a disordered normal metal has been remarked in several other instances [9, 19]. We have to point out, however, that this resemblance does not go farther in our case, regarding other regimes of the graphene Josephson junction. In particular, we have seen that the critical current does not follow an exponential decay at distances larger than the thermal length. The decay of the critical current is always given in graphene by a power law, which can be seen as a consequence of the perfect scaling of the low-energy Dirac theory.

We also have to stress that our results refer to Josephson junctions with graphene layers which have large dimensions in both the longitudinal direction along the junction and the transverse direction. This condition comes from our consideration of a system which is truly 2D, where in particular the size in the direction transverse to the junction is not constrained by the width of the superconducting contacts. In this regard, the situation is quite different to the case of long but narrow junctions, where the small transverse dimension may lead to the quantization of the transverse component of the momentum. In such circumstances, the behavior of the system may be rather dictated by a 1D propagation of the Cooper pairs, which is known to lead to a $1/L$ decay of the supercurrents in the ballistic regime [22, 26].

Anyhow, the great advantage of the graphene Josephson junctions is that the interaction effects have little significance at the temperatures required to measure the supercurrents. In the long 1D junctions made of carbon nanotubes, for instance, it is known that the Coulomb interaction may induce a strong power-law suppression of the density of states, with the consequent reflection in the decay of the supercurrent [26]. In 2D graphene, however, the electron system has the tendency to become less correlated at low energies, with a strong renormalization of the Coulomb interaction that makes it practically irrelevant at the temperature scale of 1 K [24, 29].

In conclusion, our results highlight the role of the different parameters conforming the geometry of graphene Josephson junctions in the determination of the critical currents. We have seen that the interplay with variables like the temperature and the doping level is what establishes the different regimes of a junction. This information may be useful in the design of experiments, for the purpose of enhancing the magnitude of the critical currents in real devices.

Acknowledgments

We thank H Bouchiat and F Guinea for useful comments. The financial support of the Ministerio de Educación y Ciencia

(Spain) through grant FIS2005-05478-C02-02 is gratefully acknowledged. EP is also financially supported by CNISM (Italy).

Appendix

A.1. Lowest-order contribution to the critical current

The Josephson current I_s can be computed in a perturbative framework by expanding the free energy in equation (3) in powers of the tunneling amplitude t. The first nonvanishing contribution is found to fourth order in this expansion, as the statistical average of operators leads then to the appearance of the condensates of the two superconductors in the junction. We have actually

$$\begin{aligned} I_s \approx 2e\frac{\partial}{\partial\chi}k_{\mathrm{B}}T\, t^4 \prod_{i=1}^{4}\int_0^{1/k_{\mathrm{B}}T} \mathrm{d}\tau_i \\ \times \int_0^W \mathrm{d}y_i\, \langle \Psi_{S1,\uparrow}(0,y_1;-\mathrm{i}\tau_1)\Psi_{S1,\downarrow}(0,y_2;-\mathrm{i}\tau_2)\rangle \\ \times \langle \Psi_{\uparrow}^{(a)\dagger}(0,y_1;-\mathrm{i}\tau_1)\Psi_{\downarrow}^{(-a)\dagger}(0,y_2;-\mathrm{i}\tau_2) \\ \times \Psi_{\uparrow}^{(b)}(L,y_3;-\mathrm{i}\tau_3)\Psi_{\downarrow}^{(-b)}(L,y_4;-\mathrm{i}\tau_4)\rangle \\ \times \langle \Psi_{S2,\uparrow}^{\dagger}(L,y_3;-\mathrm{i}\tau_3)\Psi_{S2,\downarrow}^{\dagger}(L,y_4;-\mathrm{i}\tau_4)\rangle. \end{aligned} \tag{30}$$

We can apply to equation (30) the approximations pertinent to the regime we want to study in the paper. Focusing on the case of a large junction where the distance L is much larger than the superconducting coherence length ξ, the use of equation (4) and translational invariance in the variable τ leads to a maximum supercurrent I_{c} (critical current)

$$\begin{aligned} I_{\mathrm{c}}(T) \approx 2e\rho^2 t^4 W^2 \prod_{i=1}^{2}\int_0^W \mathrm{d}y_i \\ \times \int_0^{1/k_{\mathrm{B}}T} \mathrm{d}\tau\, \langle \Psi_{\uparrow}^{(a)\dagger}(0,y_1;0)\Psi_{\downarrow}^{(-a)\dagger}(0,y_1;0) \\ \times \Psi_{\uparrow}^{(b)}(L,y_2;-\mathrm{i}\tau)\Psi_{\downarrow}^{(-b)}(L,y_2;-\mathrm{i}\tau)\rangle. \end{aligned} \tag{31}$$

At this point, it becomes convenient to factor out the relative tunnel conductances at the contacts, which are each given by the dimensionless quantity $\rho t^2 W/v_{\mathrm{F}}$. We concentrate then on the behavior of the critical current intrinsic to the 2D graphene system, represented by the expression

$$\begin{aligned} I_{\mathrm{c}}^{(2\mathrm{D})}(T) \approx 2ev_{\mathrm{F}}^2 \int_0^W \mathrm{d}y_1 \int_0^W \mathrm{d}y_2 \\ \times \int_0^{1/k_{\mathrm{B}}T} \mathrm{d}\tau\, \langle \Psi_{\uparrow}^{(a)\dagger}(0,y_1;0)\Psi_{\downarrow}^{(-a)\dagger}(0,y_1;0) \\ \times \Psi_{\uparrow}^{(b)}(L,y_2;-\mathrm{i}\tau)\Psi_{\downarrow}^{(-b)}(L,y_2;-\mathrm{i}\tau)\rangle. \end{aligned} \tag{32}$$

This last equation highlights the connection between the critical current and the propagator of the Cooper pairs, which plays a central role in the discussion of sections 3 and 4 in the paper.

A.2. Dirac propagator at $\mu \neq 0$

In the many-body theory of Dirac fermions, it is usual to write the Dirac propagator at finite charge density in the form (assuming $\mu > 0$)

$$\begin{aligned} G^{(a)}(\mathbf{k},\omega) = (\omega + v_{\mathrm{F}}\boldsymbol{\sigma}^{(a)}\cdot\mathbf{k})\Bigg[\frac{1}{\omega^2 - v_{\mathrm{F}}^2\mathbf{k}^2 + \mathrm{i}\epsilon} \\ + \mathrm{i}\pi\frac{\delta(\omega - v_{\mathrm{F}}|\mathbf{k}|)}{v_{\mathrm{F}}|\mathbf{k}|}\theta(\mu - v_{\mathrm{F}}|\mathbf{k}|)\Bigg]. \end{aligned} \tag{33}$$

If we specialize the expression (33) to modes such that the eigenvalue $\varepsilon(\mathbf{k})$ of the matrix $v_{\mathrm{F}}\boldsymbol{\sigma}^{(a)}\cdot\mathbf{k}$ is positive, we get

$$\begin{aligned} G^{(a)}(\mathbf{k},\omega)|_{\varepsilon(\mathbf{k})=v_{\mathrm{F}}|\mathbf{k}|} = \frac{1}{\omega - v_{\mathrm{F}}|\mathbf{k}|} \\ - \mathrm{i}\pi\frac{\omega + v_{\mathrm{F}}|\mathbf{k}|}{2v_{\mathrm{F}}|\mathbf{k}|}\delta(\omega - v_{\mathrm{F}}|\mathbf{k}|) \\ = \frac{1}{\omega - v_{\mathrm{F}}|\mathbf{k}| + \mathrm{i}\epsilon} \end{aligned} \tag{34}$$

for $v_{\mathrm{F}}|\mathbf{k}| > \mu$, and

$$\begin{aligned} G^{(a)}(\mathbf{k},\omega)|_{\varepsilon(\mathbf{k})=v_{\mathrm{F}}|\mathbf{k}|} = \frac{1}{\omega - v_{\mathrm{F}}|\mathbf{k}|} \\ + \mathrm{i}\pi\frac{\omega + v_{\mathrm{F}}|\mathbf{k}|}{2v_{\mathrm{F}}|\mathbf{k}|}\delta(\omega - v_{\mathrm{F}}|\mathbf{k}|) \\ = \frac{1}{\omega - v_{\mathrm{F}}|\mathbf{k}| - \mathrm{i}\epsilon} \end{aligned} \tag{35}$$

for $v_{\mathrm{F}}|\mathbf{k}| < \mu$. We observe that, in either case, the expression of $G^{(a)}(\mathbf{k},\omega)$ agrees with the conventional propagation of a fermion, with the correct $\pm\mathrm{i}\epsilon$ prescription depending on whether it corresponds to a quasiparticle or a quasihole excitation.

On the other hand, we always have in the case of negative eigenvalue $\varepsilon(\mathbf{k})$

$$\begin{aligned} G^{(a)}(\mathbf{k},\omega)|_{\varepsilon(\mathbf{k})=-v_{\mathrm{F}}|\mathbf{k}|} = \frac{1}{\omega + v_{\mathrm{F}}|\mathbf{k}|} \\ - \mathrm{i}\pi\frac{\omega - v_{\mathrm{F}}|\mathbf{k}|}{2v_{\mathrm{F}}|\mathbf{k}|}\delta(\omega + v_{\mathrm{F}}|\mathbf{k}|) \\ = \frac{1}{\omega + v_{\mathrm{F}}|\mathbf{k}| - \mathrm{i}\epsilon} \end{aligned} \tag{36}$$

which is also in agreement with the expected propagation for a quasihole in the valence band of graphene.

References

[1] Novoselov K S, Geim A K, Morozov S V, Jiang D, Zhang Y, Dubonos S V, Grigorieva I V and Firsov A A 2004 *Science* **306** 666

[2] See, for instance, Geim A K and Novoselov K S 2007 *Nat. Mater.* **6** 183

[3] Novoselov K S, Geim A K, Morozov S V, Jiang D, Katsnelson M I, Grigorieva I V, Dubonos S V and Firsov A A 2005 *Nature* **438** 197

[4] Zhang Y, Tan Y-W, Stormer H L and Kim P 2005 *Nature* **438** 201

[5] Morozov S V, Novoselov K S, Katsnelson M I, Schedin F, Ponomarenko L A, Jiang D and Geim A K 2006 *Phys. Rev. Lett.* **97** 016801

[6] Wallace P R 1947 *Phys. Rev.* **71** 622

[7] Peres N M R, Guinea F and Castro Neto A H 2006 *Phys. Rev.* B **73** 125411

[8] Katsnelson M I 2006 *Eur. Phys. J.* B **51** 157

[9] Tworzydlo J, Trauzettel B, Titov M, Rycerz A and Beenakker C W J 2006 *Phys. Rev. Lett.* **96** 246802

[10] Nomura K and MacDonald A H 2007 *Phys. Rev. Lett.* **98** 076602
[11] Zheng Y and Ando T 2002 *Phys. Rev.* B **65** 245420
[12] Gusynin V P and Sharapov S G 2005 *Phys. Rev. Lett.* **95** 146801
[13] Suzuura H and Ando T 2002 *Phys. Rev. Lett.* **89** 266603
[14] Cheianov V V and Fal'ko V I 2006 *Phys. Rev.* B **74** 041403
[15] Beenakker C W J 2006 *Phys. Rev. Lett.* **97** 067007
[16] Heersche H B, Jarillo-Herrero P, Oostinga J B, Vandersypen L M K and Morpurgo A F 2007 *Nature* **446** 56
[17] Shailos A, Nativel W, Kasumov A, Collet C, Ferrier M, Guéron S, Deblock R and Bouchiat H 2007 *Europhys. Lett.* **79** 57008
[18] Du X, Skachko I and Andrei E Y 2007 *Preprint* cond-mat/0710.4984
[19] Titov M and Beenakker C W J 2006 *Phys. Rev.* B **74** 041401(R)
[20] DiVincenzo D P and Mele E J 1984 *Phys. Rev.* B **29** 1685
[21] González J, Guinea F and Vozmediano M A H 1993 *Nucl. Phys.* B **406** 771
[22] Fazio R, Hekking F W J and Odintsov A A 1996 *Phys. Rev.* B **53** 6653
[23] Dolan L and Jackiw R 1974 *Phys. Rev.* D **9** 3320
[24] González J, Guinea F and Vozmediano M A H 1994 *Nucl. Phys.* B **424** 595
[25] González J and Perfetto E 2007 *Phys. Rev.* B **76** 155404
[26] González J 2001 *Phys. Rev. Lett.* **87** 136401
González J 2003 *J. Phys.: Condens. Matter* **15** S2473
[27] See, for instance, Chin S A 1977 *Ann. Phys.* **108** 301
[28] Dubos P, Courtois H, Pannetier B, Wilhelm F K, Zaikin A D and Schön G 2001 *Phys. Rev.* B **63** 064502
[29] González J, Guinea F and Vozmediano M A H 1999 *Phys. Rev.* B **59** R2474